Water Research 165 (2019) 115016

Contents lists available at ScienceDirect

Water Research

journal homepage: www.elsevier.com/locate/watres

Co-doping polymethyl methacrylate and copper tailings to improve the performances of sludge-derived particle electrode

Hui-shan Meng [a], Chen Chen [a], Zi-run Yan [a], Xiu-yan Li [a], Juan Xu [a, b, *], Guo-ping Sheng [c]

[a] Shanghai Key Lab for Urban Ecological Processes and Eco-Restoration, School of Ecological and Environmental Sciences, East China Normal University, Shanghai, 200241, China
[b] Institute of Eco-Chongming (IEC), No.20 Cuiniao Road, ChenJiazhen, Shanghai, 202162, China
[c] CAS Key Laboratory of Urban Pollutant Conversion, School of Chemistry and Materials Science, University of Science and Technology of China, Hefei, 230026, China

ARTICLE INFO

Article history:
Received 28 March 2019
Received in revised form
9 August 2019
Accepted 19 August 2019
Available online 21 August 2019

Keywords:
Hierarchical-pore
Particle electrode
Three-dimensional electrochemical reactor
Waste sludge
Wastewater treatment

ABSTRACT

Three-dimensional electrochemical reactor (3DER) is a highly efficient technology for refractory wastewater treatment. Particle electrodes filled between anode and cathode are the core units of 3DER, determining the treatment efficiency of wastewater. However, particle electrodes deactivation due to catalytic sites coverage seriously impedes the continuous operation of 3DER. In this work, granular sludge carbon (GSC) particle electrodes being resistant to deactivation are fabricated by pyrolyzing the mixture of waste sludge, polymethyl methacrylate (PMMA), and copper tailings, whose performances are evaluated by degrading rhodamine B (RhB) wastewater in a continuous-flow 3DER. Results indicate that hierarchical-pore structure comprising macro-, meso-, and micropores is developed in GSC-10-CTs by doping 10 g PMMA and 5 g copper tailings into 100 g waste sludge. PMMA contributes to construct macropores, which is essential for the mass transfer of RhB into GSC particle electrodes of centimeter-size. Copper tailings promote the formation of meso- and micro-pores in GSCs, as well as improving the electrochemical properties. Consequently, GSC-10-CTs packed 3DER exhibits the highest removal efficiency and lowest energy consumption for RhB treatment. In addition, the compressive strength of GSC-10-CTs is enhanced by copper tails, that is crucial to fill into 3DER as particle electrodes. The high-efficient and cost-effective GSC-10-CTs fabricated by waste materials have the potential of substituting commercial granular activated carbon catalysts in the future, consequently promoting the application of 3DER in wastewater treatment.

1. Introduction

Treatment of industrial refractory wastewater is a great challenge in China. Various physical-chemical approaches have been applied to deal with these wastewater, among which three-dimensional electrochemical reactor (3DER) is a highly efficient and environmental friendly technology (Zheng et al., 2016). Based on conventional electrochemical technology, 3DER is developed by filling conductive particles such as granular activated carbon (GAC) between anode and cathode (Wei et al., 2010). After applying external electric field, these particles are polarized to be multiple microelectrodes, significantly improving the efficiency of wastewater treatment. GAC is the most widely used particle electrodes due to its good electrical conductivity, large surface area and low cost. Since the electrocatalytic activity of pristine GAC is relatively weak, noble metals such as Pd and Cu are loaded onto GAC to enhance its electrocatalytic property (Zhang et al., 2013). Some metal oxides (Fe_3O_4, SnO_2, Sb_2O_3, RuO_2, IrO_2) supported GACs also exhibit high electrocatalytic activity (Li et al., 2016). However, deactivation of GAC catalysts due to the coverage of catalytic sites by contaminants seriously deteriorates the treatment performance of 3DER during long-term operation. Furthermore, the expense of GAC catalysts are too expensive for wastewater treatment. Therefore, particle electrodes of high-efficient and cost-effective are still in urgent need by 3DER technology.

Currently, multifunctional carbon materials converted from waste sludge exhibit potential in electrochemical energy storage

* Corresponding author. Shanghai Key Lab for Urban Ecological Processes and Eco-Restoration, School of Ecological and Environmental Sciences, East China Normal University, Shanghai, 200241, China.
E-mail address: jxu@des.ecnu.edu.cn (J. Xu).

https://doi.org/10.1016/j.watres.2019.115016
0043-1354/

and pollutants adsorption/catalytic oxidation (Yuan and Dai, 2016). Particularly, waste sludge derived carbons (SCs) are used as electrocatalysts for their carbonaceous nature and co-existence of metal elements. Acid orange 7 dyeing wastewater can be degraded by 80.2% through the electrocatalysis of SCs powder (Sun et al., 2015). Iron oxide supported SCs powder has the capability of purifying coal gasification wastewater by electrochemical oxidation (Hou et al., 2016). Although the efficacy of SCs powder is verified, the difficulties in separating and recovering powder catalysts restrain the practical application of SCs. Therefore, granular sludge carbon (GSCs) is fabricated and successfully applied as particle electrodes of 3DER to treat dyeing wastewater in our previous work (Ji et al., 2018). GSCs is demonstrated to be highly efficient initially, but the treatment performance of 3DER is inevitably attenuating during the continuous operation ascribing to the deactivation of GSCs. Since contaminants adsorption at the interface of GSCs is more rapid than contaminants decomposition by electrocatalysis, the active catalytic sites are gradually covered by the accumulated contaminants. To maintain a stable treatment performance, the structure of GSCs should be optimized to balance the processes of adsorption and electrocatalysis.

The adsorption property of GSCs is highly dependent on porous structure, which can be regulated by adding pore-forming agents (Kong et al., 2013). The electrocatalytic property of GSCs can be improved by optimizing catalytic components. Therefore, polymethyl methacrylate (PMMA) and waste copper tailings are doped into waste sludge to improve the performances of GSCs in present work. PMMA is a spherical plastic particle that easily burned out during pyrolysis (Xia et al., 2011), consequently creating multiple pores in GSCs. Porous structure of GSCs is designed to enhance the mass transfer between contaminants and GSCs particle electrodes, promoting adsorption and electrocatalysis occurred in 3DER. Copper tailings comprise various metal components such as Cu and Fe, which can improve the electrocatalytic activity of GSCs (Thomas et al., 2013). The synergy of adsorption and electrocatalysis would effectively relieve the coverage of active catalytic sites in GSCs, and achieve a stable treatment performance in 3DER.

In this study, GSCs particle electrodes being resistant to deactivation were fabricated by pyrolyzing the mixture of waste sludge, PMMA, and copper tailings. The performances of the prepared GSCs were evaluated by degrading rhodamine B (RhB) wastewater in a continuous-flow 3DER. The roles of PMMA and copper tailings in improving the properties of GSCs were investigated, from the aspects of porous structure and electrocatalytic activity of the materials. Herein, we report a strategy of fabricating porous GSCs as high-efficient and cost-effective particle electrodes, consequently promoting the application of 3DER in wastewater treatment.

2. Materials and methods

2.1. Materials and reagents

The dewatered waste sludge obtained from Tianshan wastewater treatment plant (Shanghai, China) was pretreated with $FeSO_4$ and $Ca(OH)_2$. Copper tailings were collected from the mineral processing slag of a copper mine located in Tongling, Anhui, China. Waste sludge contained abundant C (26.58%), Ca (32.16%) and Fe (19.12%) elements (Table S1). Copper tailings comprised various metal elements such as Fe (32.33%) and Cu (0.88%). Waste sludge and copper tailings were ground into fine powder of less than 150 mesh before utilization. PMMA with the average particle size of 10 μm were purchased from Mitsubishi Co., Guangdong, China. The other regents are all analytical grade from Sinopharm Co., Shanghai, China.

2.2. Preparation of GSCs

The GSCs were fabricated referring to our previous work with a few modifications (Ji et al., 2018). 100 g sludge powder was mixed with $ZnCl_2$ solution (40 wt%) as activation agent and 1 g sodium carboxymethyl cellulose as adhesive. The mixture was stirred slowly for 12 h at ambient temperature, and then was shaped into spherical precursors with the diameter of 8 mm by a granulator (LD-88A, Chuangli, China). The obtained particles were dried at 105 °C for 12 h and subsequently pyrolyzed in a tube furnace (GSL-1400X, Kejing, China) at heating rate of 10 °C/min to 600 °C in the presence of N_2 holding for 2 h. After cooling down, the products were washed with 80 °C distill water until the effluent pH was constant. The obtained particles were dried at 105 °C overnight and labeled as GSC. PMMA and copper tailings were doped into the sludge powder before activation to improve the performances of GSC. The dosages of PMMA and copper tailings were optimized previously as described in Supplementary Materials. To investigate the roles of PMMA and copper tailings as well as the synergy of the two additives in GSC improvement, different fabrication conditions were selected as listed in Table 1.

2.3. Analytical methods

Themogravimetric (TG) analysis was carried on a thermogravimetric analyzer (TGA/SDTA851e, Mettler toledo, Switzerland). Compressive strength of GSCs was measured by an automatic particle strength tester (YHKC-3A, Jiangyan, China). The conductivity of GSCs were measured by four-point probe method on a resistivity meter (ST2722-SZ, Suzhou Jingge Electronics, China). The bulk chemical compositions of GSCs were determined via an X-ray fluorescence spectrometer (XRF, Axios, PANalytical, Netherlands). Microscopic structure of GSCs were observed by a scanning electron microscope (SEM, HITACHI S-4800, HSD, Japan). The pore characteristics of GSCs were investigated combining nitrogen adsorption (Auto-sorb-6, Quantachrome, USA) and mercury intrusion method (AutoPore IV 9500, Micromeritics Instrument, UAS). The crystal structure of GSCs was analyzed on a powder X-ray diffractometer (XRD, Ultima-IV, Rigaku, Japan). Chemical species of Zn, Fe, C, and O in GSCs were analyzed by X-ray photoelectron spectroscopic patterns (XPS, Escalab 250Xi, Thermo, USA). RhB was utilized as a target contaminant, being quantified by a UV−visible spectrophotometer at the wavelength of 554 nm (MAPADA, China). Radicals generated during the treatment process were detected by electron spin resonance (ESR, EMX-8/2.7, Bruker, Germany).

The electrochemical properties of GSCs were analyzed on an electrochemical workstation (CHI 660E, Chenhua, China) using a three-electrode system. A glassy carbon disk (3.0 mm in diameter) coated with various GSCs was used as the working electrode, with Pt wire as the counter electrode and Ag/AgCl electrode as the reference electrode (Ji et al., 2018). The cyclic voltammetry (CV) measurements were conducted in RhB and $K_4Fe(CN)_6$ solution, respectively. Electrochemical impedance spectroscopy (EIS) were measured in $K_3Fe(CN)_6$ solution. N_2 was purged into the solution for 30 min prior to each scan.

Table 1
Ratios of sludge, PMMA and copper tailings for fabricating different GSCs.

Samples	Sludge (g)	PMMA (g)	Copper tailings (g)
GSC	100	0	0
GSC-10	100	10	0
GSC-CTs	100	0	5
GSC-10-CTs	100	10	5

2.4. Continuous-flow 3DER for evaluating the performances of GSCs

The configuration of the continuous-flow 3DER was displayed in Fig. 1, which was a plexiglas rectangular tank with the working volume of 80 mL. Two main electrodes including a Ti/RuO_2−IrO_2 anode (100 × 30 × 1 mm) and a titanium plate cathode with the same dimension (Shuerde Co., China) were positioned vertically and parallel to each other with an inner gap of 3 cm. The prepared GSCs of 40 g were filled between anode and cathode. Commercial GAC catalysts (Jiacheng Co., Zhejiang, China) and 2DER without particle electrodes were also tested for comparison. The concentration of RhB in influent was 50 mg/L with 0.1 M Na_2SO_4 electrolyte. The flow rate of influent was 6.67 mL/min, corresponding to a hydraulic retention time (HRT) of 12 min. Air was sparged into 3DER through the air inlet (Fig. 1) to promote mass transfer and pollutants degradation (Zhang et al., 2013). The air inlet was connecting with an aeration pump, and the aeration rate was maintained at 15 mL/min by adjusting the flow meter. The concentration of oxygen in 3DER was determined to be 8.15 mg/L by a dissolved oxygen meter (HQ30d, HACH, USA). Magnetic stirring was carried at the bottom of the reactor to enhance mass transfer of oxygen into RhB solution (Contreras Moreno et al., 2017), and to improve the electrocatalytic reactions at gas-liquid-solid (oxygen-RhB-particle electrodes) three-phase interfaces in 3DER (Fig. S1). RhB was pumped into the 3DER continuously, and voltage (8 V) was provided by a digital DC power supply (CE0036030S, RainWorm, China). The experiments of RhB degradation in 3DER were carried out at the room temperature of 26 °C. The effluent samples were collected and filtered through 0.45 μm nitrocellulose membrane before analysis.

Energy consumption (EC, kWh/g RhB) of 3DER was calculated as follows (Neti and Misra, 2012).

$$EC = \frac{UI}{(C_0 - C_t) \times Q} \quad (1)$$

where U is the applied voltage (V), I is the current (A), C_0 is the initial RhB concentration (mg/L), C_t is RhB concentration at time t (mg/L), Q is the flow rate of RhB solution (L/h).

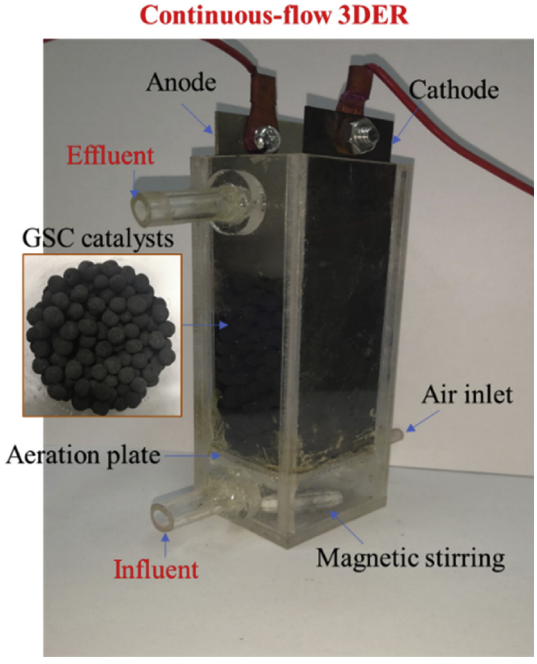

Fig. 1. Configuration of the continuous-flow 3DER for RhB degradation.

3. Results

3.1. Wastewater treatment performance of 3DER filled with GSCs

The removal efficiency of RhB in continuous-flow 3DER is shown in Fig. 2a. The average removal efficiency was only 24.2% for 2D system in the absence of GSCs. The removal efficiency attenuated from 79.1% to 56.2% in 14 h when filling commercial GAC catalysts in 3DER. Remarkable improvement in RhB removal efficiency was observed for 3DER filled with prepared GSCs particle electrodes. For GSC, the removal efficiency maintained over 90% during the initial 6 h, while decreasing to 52.9% when the treatment time prolonged to 14 h. For GSC-CTs, the removal efficiency was slightly higher than GSC during the initial 8 h, while decreasing more rapidly to 38.9% in 14 h. Doping 10% PMMA (GSC-10) significantly enhanced the removal efficiency in the first 8 h, and the average removal efficiency was as high as 98.9%. However, the removal efficiency decreased quickly to 47.2% in the late 6 h. For GSC-10-CTs, the removal efficiency was relatively stable ranging from 85.4% to 99.6%. The removal efficiency maintained over 94.1% during 12 h operation, then decreased by less than 10% in the late 2 h. Apparently, GSC-10-CTs were more resistant to deactivation compared to the other GSCs, achieving a durable treatment performance in 14 h. What's more, the dissolution of Cu and Fe species from GSC-10-CTs into the effluent were negligible during the treatment process (Table S2), suggesting the stability of the prepared GSC-10-CTs.

Current is another important parameter to characterize the electrocatalytic process in 3DER. Current for all the GSCs were relatively stable during the treatment process in the presence of 8 V voltage (Fig. 2c). 2D system generated the highest current value. The current was lower for 3DER filled with GSCs compared to 3DER filled with commercial GAC catalysts. The lowest current presented when GSC-10-CTs was filled in 3DER for RhB treatment. Energy consumption (EC) directly determined the operation cost of 3DER. Fig. 2d indicated that 2D system consumed much more electric energy than 3DER. For commercial GAC catalysts, EC increased slightly with the prolonging treatment time. EC of GSC-CTs was lower than that of commercial GAC catalysts in the first 9 h, but gradually approaching even exceeding that of commercial GAC catalysts after 12 h. EC of GSC, GSC-10 were lower than that of commercial GAC catalysts, while slightly increased after 10 h. It was noticed that EC of GSC-10-CTs was the lowest and maintained stable during the whole 14 h treatment. The results also verified the impressive performance of GSC-10-CTs in energy consumption, as well as the highest removal efficiency.

The superiority of GSC-10-CTs was ascribed to hierarchical-pore structure and better electrocatalytic properties.

3.2. Porous structure of GSCs

GSCs particle electrodes taken effect on RhB removal in 3DER by adsorption and electrocatalysis. The adsorption capability of the GSCs made considerable contributions to RhB removal, as shown in Fig. 2b. The adsorption property of GSCs followed the order of GSC-10>GSC-10-CTs > GSC > GSC-CTs. It was clearly that PMMA addition enhanced RhB adsorption while doping copper tailings was to the opposite. However, when looking over the BET surface area of GSCs (Table 2), GSC-10 had the lowest surface area of 56.55 m^2/g. The adsorption property of GSCs was independent on the surface area. The results revealed that the adsorption behavior of GSCs in 3DER was different from that of the powder materials. Adsorption of RhB highly relied on the macropores in GSCs, which existed in GSC-10 GSC-10-CTs due to PMMA dosage.

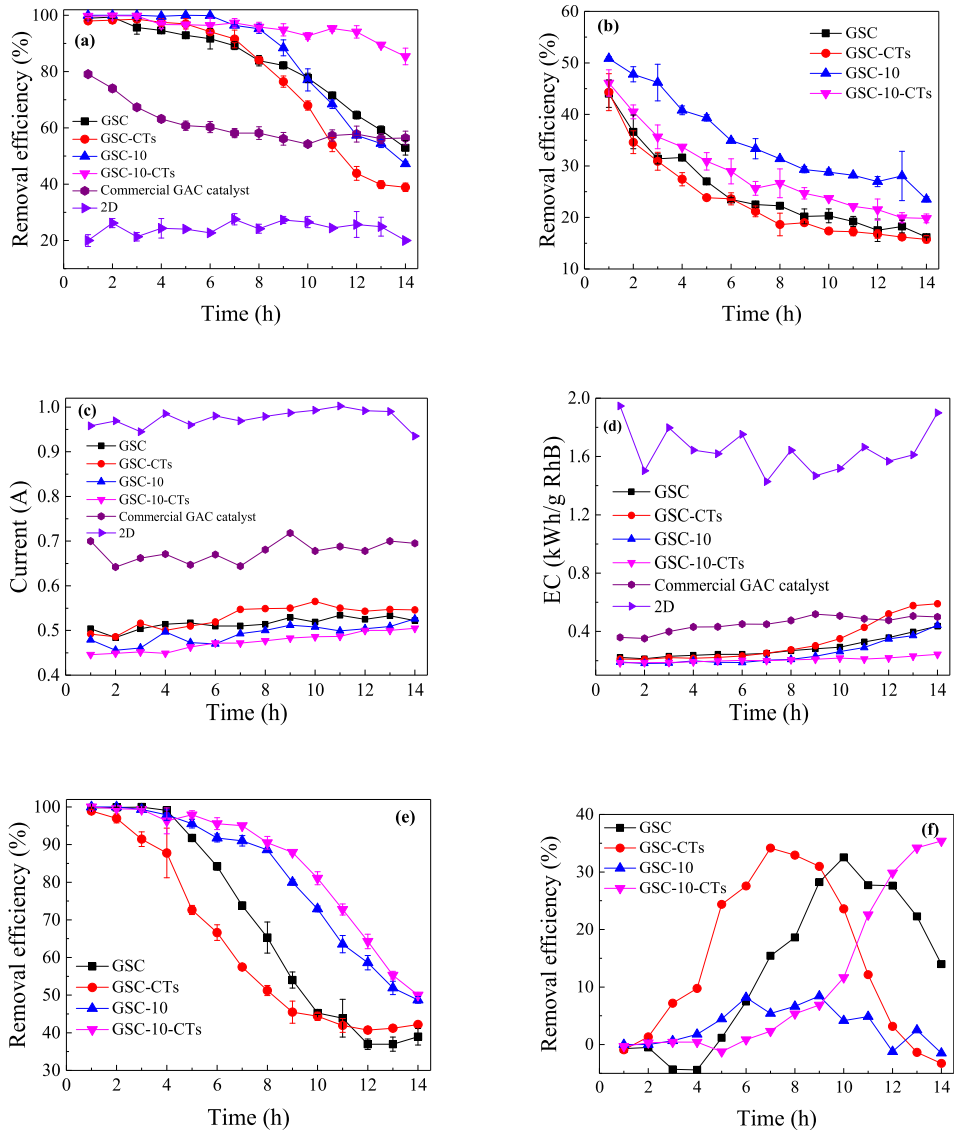

Fig. 2. RhB removal in the continuous-flow 3DER filled with different GSCs (a) applying 8 V voltage; (b) without external voltage; (c) current variation; (d) energy consumption; (e) in the presence of tertbutyl alcohol radical scavengers; (f) the contribution of radicals to RhB removal efficiency by subtracting (a) to (e).

Table 2
Physical and chemical properties of the GSCs.

Samples	C (%)	H (%)	N (%)	S (%)	Fe (%)	Zn (%)	Cu (%)	Ash (%)	Yield (%)	Apparent Density (g/mL)	Compressive strength (N)	Conductivity ($\times 10^4$ S/cm)	Surface area (m^2/g)	Pore volume (cm^3/g)
GSC	14.09	1.42	1.26	0.88	13.79	49.09	0.070	78.85	67.30	0.64	20.82	0.047	114.40	0.24
GSC-10	18.36	1.46	1.20	0.88	14.25	46.73	0.070	69.24	60.40	0.51	13.70	0.35	56.55	0.14
GSC-CTs	12.89	1.26	1.02	1.14	14.64	44.67	0.46	84.55	65.90	0.62	35.55	1.57	88.01	0.21
GSC-10-CTs	21.51	1.42	1.3	1.48	18.46	41.88	0.57	72.47	58.34	0.49	19.64	0.63	99.39	0.15

Thermal analysis in Fig. S2 confirmed the pore-forming capability of PMMA. GSC-10 precursor mainly experienced a three-stage weight loss. The first stage ranged from 25 to 200 °C, which was due to the release of moisture and decomposition of volatile organics (Bandosz and Block, 2006). The majority of the weight loss occurred between 200 and 600 °C, which was related to the vaporization of PMMA and organics such as proteins, carbohydrates and aliphatic compounds (Li et al., 2018). There was slight weight loss at the final stage of 600–700 °C, owing to the hardly decomposable substance. Since PMMA started to burn out at 400 °C, GSC-10 precursor had more dramatic weight loss compared to GSC precursor due to vaporization of PMMA when temperature increased over 400 °C. The results demonstrated the capability of PMMA in fabricating macropores during the pyrolysis of waste sludge.

SEM in Fig. 3 displayed the morphology and porous structure of GSCs. GSC surface was relatively dense without obvious pores. The

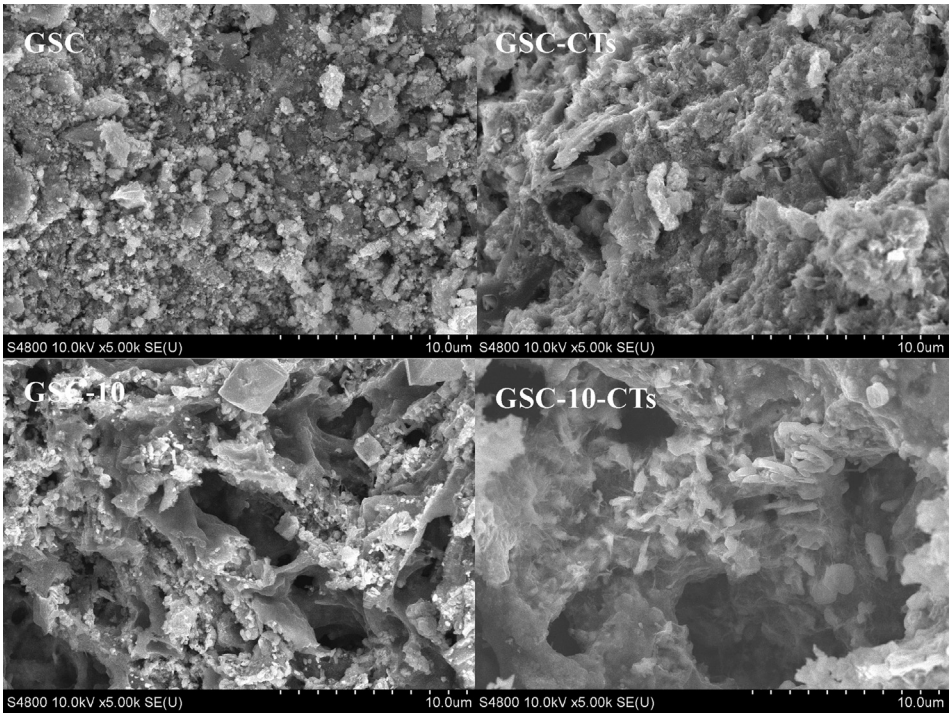

Fig. 3. SEM images of the GSCs.

surface of GSC-CTs were rougher compared to that of GSC, with development of noticeable pores. That might be related to the inorganic components such as Fe and Cu in the doped copper tailings (Table S1), which were used to develop porous structure in sludge-based adsorbents (Xie et al., 2013). Therefore, copper tailings also exhibited the capability of fabricating pores in GSCs. Large pores over 10 μm in GSC-10 was fabricated by vaporization of PMMA (10–11 μm) during pyrolysis. The pores were further enlarged in GSC-10-CTs. In addition, flake-like crystals grew both on the surface and at the pores wall of GSC-10-CTs. Accordingly, PMMA mainly contributed to developing macropores while copper tailings promoted the formation of porous structure and deposition of crystals.

N_2 adsorption-desorption isotherms for the prepared GSCs (Fig. S3) exhibited type IV isotherm of IUPAC definition (Lee et al., 2013). Hysteresis loop over a wide relative pressure ranging from 0.4 to 1.0 suggested the existence of mesopores in all the GSCs. H3 hysteresis loops associated with GSC and GSC-CTs revealed wedge-shaped pores (East, 2016). H4 hysteresis loop indicated the micro-mesoporous structure of GSC-10 and GSC-10-CTs (Feng et al., 2015). Abundant Fe components in sludge promoted the development of the porous structure of the GSCs. Li et al. reported that adding scrap iron comprising Fe, Fe_2O_3, and Fe_3O_4 into sewage sludge significantly improved the formation of mesopores in the produced activated carbon (Li et al., 2015). Yang et al. found that Fe_2O_3 in-situ catalyzed the cracking of C–C and C–H bonds in tar to produce porous structure of sewage sludge (Yang et al., 2018). Ferric salts was considered to enlarge the pore volume of sludge based adsorbents by increasing mesopores (Yang et al., 2016). In this study, Fe components in raw sludge mainly presented in the forms of ferric salts and iron oxides, hence facilitating the formation of mesopores in GSCs during pyrolysis. Ca species in the sludge also contributed to the porous structure in GSCs. Liu et al. reported that Ca was favorable for the formation of pores by encouraging partial cleavages of C–C bonds and C–H bonds in the sludge, resulting in the decomposition of organic macromolecules into relative small molecules (Liu et al., 2013). In addition, porosity was also developed during volatilization of $ZnCl_2$, and additional micro-porosity and meso-porosity could arise during the washing step of removing entrapped $ZnCl_2$ (Hadi et al., 2015).

The distribution curves of pore size further figured out the porous structure of the prepared GSCs (Fig. 4). GSC exhibited broad distribution in mesopores with the diameter of 4–8 nm. GSC-CTs possessed a lower pore size distribution over 4–6 nm than GSC. Apparently, the portion of macropores in GSCs increased with PMMA doping. The obvious peak of macropores at 6 μm appeared in GSC-10. For GSC-10-CTs, macropores of 12 μm and micropores of 1.5 nm emerged. Compared to GSC-10, the enlargement of macropores in GSC-10-CTs was probably due to magnified vaporization of PMMA by inorganic components in copper tailings (Tang et al., 2018a). The micropores in GSC-10-CTs was intensified by co-doping PMMA and copper tailings, as micropores also presented in GSC-10 (Fig. S3).

3.3. Electrocatalytic activity of the GSCs

The electrochemical property of prepared GSCs was evaluated by CV measurement with 20 consecutive cycles of scan in RhB and $K_4Fe(CN)_6$ solution, respectively. As shown in Fig. 5a, obvious redox peaks of RhB were observed for all GSCs with two oxidative peaks and two reductive peaks. GSC-10-CTs exhibited the highest oxidative peak current (2.55, 2.70 mA), followed by GSC-CTs (2.39, 2.26 mA), GSC-10 (2.10, 2.24 mA) and GSC (1.63, 1.92 mA). The results indicated that the electrochemical oxidation of RhB on GSC-10-CTs and GSC-CTs was faster than on the other two GSCs. Moreover, redox reaction of $Fe(CN)_6^{4-}/Fe(CN)_6^{3-}$ on GSCs were measured (Fig. 5b). The redox peaks were quite weak for GSC-10, but obvious for the other GSCs. For GSC, there were redox peaks of $Fe(CN)_6^{4-}/Fe(CN)_6^{3-}$ with a peak separation (ΔEp) of 0.45 mV. The reduced △Ep for GSC-10-CTs and GSC-CTs suggested the declined

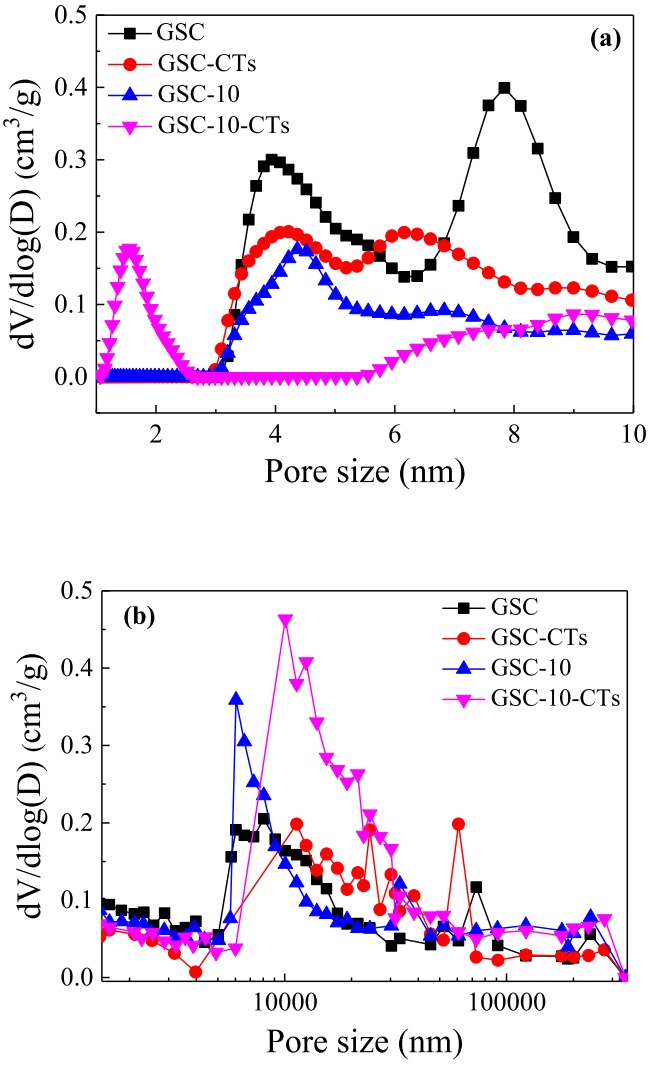

Fig. 4. Pore size distribution of the GSCs: (a) microporous and mesoporous structure by N_2 adsorption-desorption measurement; (b) macroporous structure by mercury intrusion measurement.

thermodynamic barrier of redox reactions on these two materials. Furthermore, the peak currents for GSC-10-CTs significantly increased than GSC-CTs, indicating that electron transfer rate on GSC-10-CTs was more rapid than on GSC-CTs.

The interfacial electron-transfer properties of different GSCs were evaluated by EIS measurement, with the Nyquist plots in Fig. 5c. The diameter semicircle in the high frequency range was assigned to the charge-transfer resistance (Rct) at the interface of GSCs during electrocatalysis process. Based on equivalent circuit models, (Xu and Song, 2015), the Rct values of both GSC-CTs (208.0 Ω) and GSC-10-CTs (204.0 Ω) were reduced by doping copper tailings, in comparison with GSC (217.9 Ω) and GSC-10 (258.6 Ω). The metal components such as Cu from copper tailings (Table S1) accelerated the charge-transfer reaction. The straight line in the low frequency range represented diffusion resistance of the electrode-electrolyte interface. The higher slope of linear part for GSC-10-CTs and GSC-CTs corresponded to faster diffusion rate of the electrode-electrolyte interface. Accordingly, interfacial electron-transfer properties of GSCs were improved by doping copper tailings, including both diffusion at the electrode-electrolyte interface and charge-transfer at the electrode interface. The results were in agreement with the higher conductivity of GSC-10-CTs and GSC-CTs in Table 2. Combined with CV analysis, GSC-10-CTs was demonstrated to have the highest electrochemical activity, which was essential for electrocatalysis.

3.4. Physical and chemical properties of GSCs

The physical and chemical properties of GSCs were listed in Table 2. Addition of PMMA into sludge led to a lower yield due to vaporization of PMMA during pyrolysis. The apparent density decreased with PMMA addition, demonstrating the formation of porous structure in GSCs by sacrificing PMMA templates. Accordingly, the compressive strength of the GSCs were inevitably reduced. The carbon content of GSCs increased with PMMA addition. Although pure PMMA materials completely vaporized at 400 °C (Fig. S2), mixing with sludge definitely influenced the vaporization behavior of PMMA. The presence of inherent minerals in sludge retarded the release of volatile PMMA vapors and then led to the deposition of a few PMMA (Tang et al., 2018a). Both yield and apparent density of the GSCs declined after doping copper tailings, revealing that copper tailings also contributed to the porous structure of GSCs by promoting the formation of pores in GSCs (Bagreev et al., 2001). This result confirmed the capability of copper tailings in fabricating pores, which was indicated in SEM and porosity analysis. Also, the contents of S, Fe and Cu elevated in GSCs by introducing copper tailings. Especially, the ratio of Cu, a highly efficient electrocatalytic component, increased by one magnitude after doping copper tailings. More importantly, the compressive strength of the GSCs was obviously enhanced in the presence of copper tails, that was crucial to fill GSCs into 3DER as particle electrodes for wastewater treatment.

XRD results in Fig. 6a reflected the crystal structure of the GSCs. The diffraction peak at 26.6° corresponded to the characteristic diffraction of graphite. This peak was obviously intensified and became sharper for GSCs doped with copper tailings, indicating more ordered graphite crystallites (Ji et al., 2018). Accordingly, electrochemical properties of GSCs were improved, coinciding with the increased conductivity of GSC-CTs and GSC-10-CTs in Table 2. The predominance of graphite carbon in GSCs might be ascribed to the high pyrolysis temperature of 600 °C (Gu et al., 2013; Wang et al., 2017b) and abundant Fe components in the raw sludge (Wen et al., 2018). The peaks at $2\theta = 36.2°$, 31.7°, 34.4°, 56.5°, 47.4° were the diffraction of ZnO crystalline planes, derived from $ZnCl_2$ activator. The diffraction intensity of ZnO in GSC-10-CTs declined and the shape broadened, revealing decreased crystallinity and increased distribution of ZnO (Tang et al., 2018b). That facilitated the electrocatalytic oxidation of wastewater due to more uniform catalytic sites. Fe_3O_4 ($0.5Fe^{3+}0.25Fe^{2+}O$) crystalline phase (JCPDS,89−0688) presented in GSC and GSC-10 at the pyrolysis temperature of 600 °C (Wang et al., 2017b). The diffraction intensity of Fe_3O_4 decreased with addition of copper tailings (GSC-CTs), and almost disappeared in GSC-10-CTs. Instead, diffraction peaks of wustite, i.e. $Fe_{0.95}O$ ($0.1Fe^{3+}0.85Fe^{2+}O$) (JCPDS, 79−1967) emerged in GSC-10-CTs. This was due to the reduction of Fe(III) to Fe(II) by the reductants existed in or generated from copper tailings during pyrolysis (Tang et al., 2018a). PMMA constructed macropores significantly enhanced mass transfer and more Fe(III) was exposed for reduction, leading to the accumulation of $Fe_{0.95}O$ in GSC-10-CTs. Fe(II) exhibited high catalytic activity in generating radicals (Hu et al., 2011), that were important oxidants for decomposing contaminants in 3DER. Obvious peaks of C1s, O1s, Fe2p and Zn2p were displayed in XPS spectra (Fig. 6b), corresponding to the vital components of graphite carbon, ZnO, Fe_3O_4 and $Fe_{0.95}O$ in the GSCs. High-resolution scans of Fe element (Fig. S4) indicated that both Fe(II) and Fe(III) co-existed in all the GSCs with different ratios.

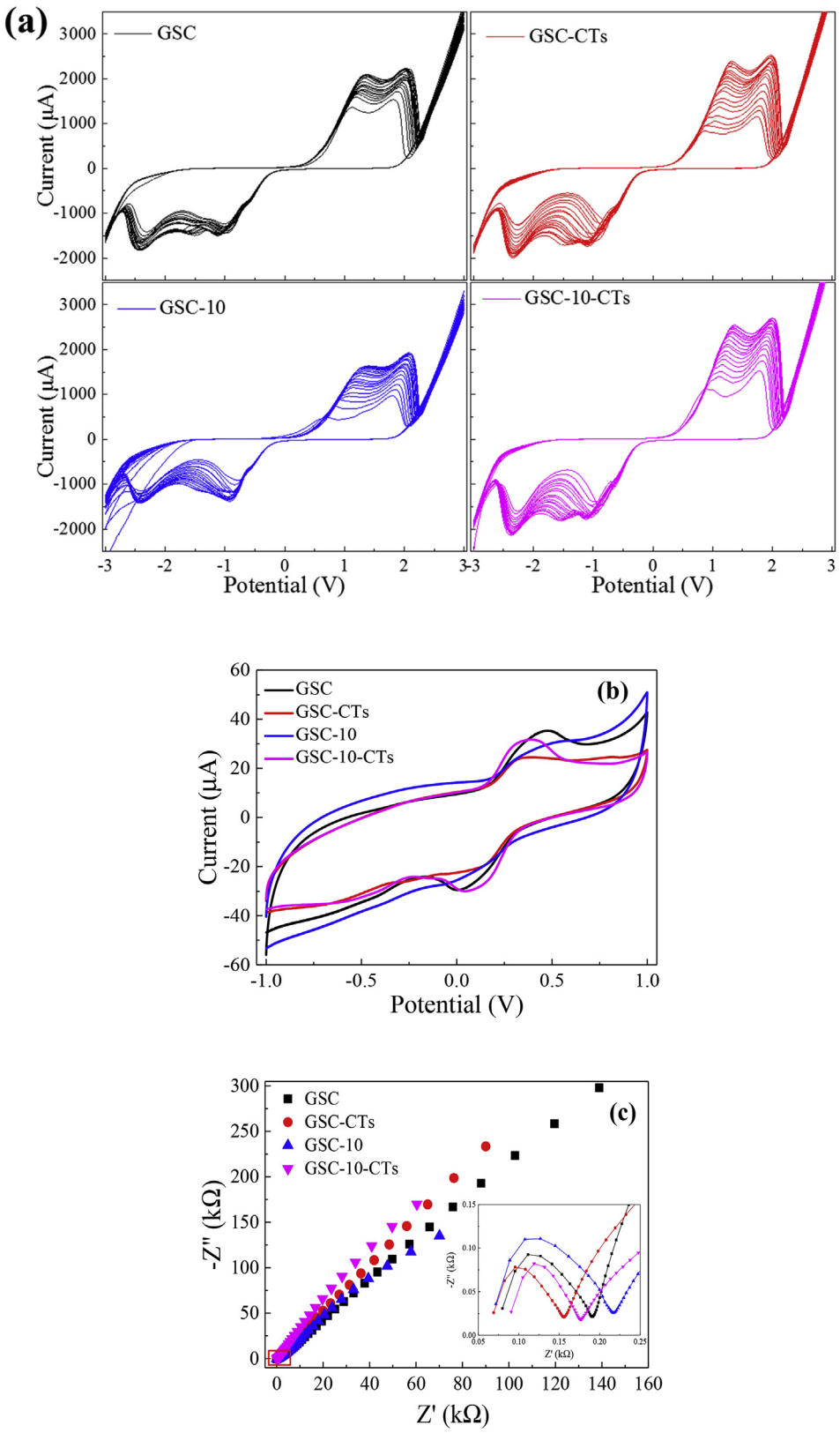

Fig. 5. (a) CVs of the GSCs recorded in 0.104 μM RhB + 0.01 M Na_2SO_4 at 0.1 V/s scan rate with 20 consecutive cycles; (b) CVs of the GSCs recorded in 5 mM $K_4Fe(CN)_6$ + 0.1 M KCl solution at 0.1 V/s scan rate; (c) EIS measurement of the GSCs recorded in 5 mM $K_3Fe(CN)_6$ + 0.1 M KCl solution, with 0.01–10^6 Hz frequency and 5 mV amplitude.

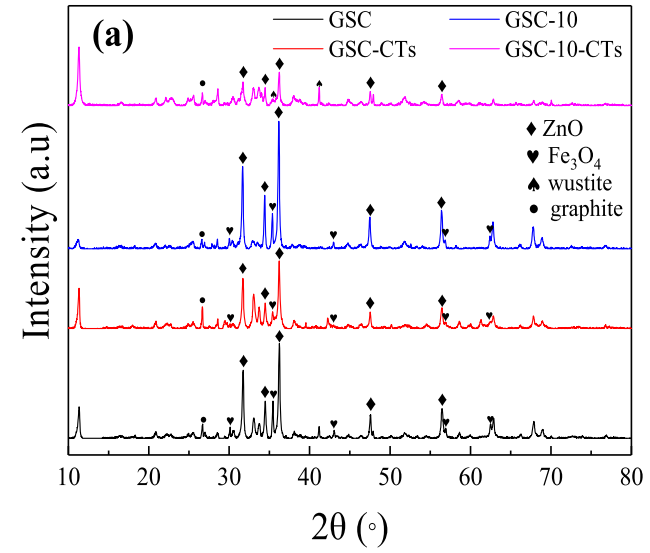

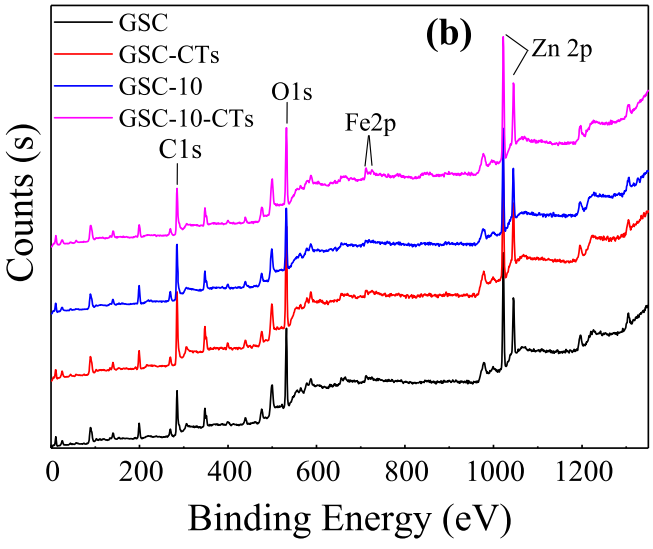

Fig. 6. (a) XRD patterns of the GSCs; (b) XPS spectra of the GSCs.

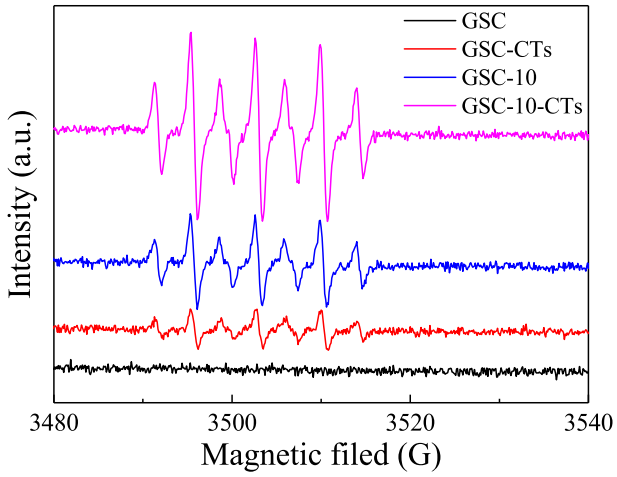

Fig. 7. ESR signals for radicals generated by the GSCs.

4. Discussion

4.1. Roles of radicals in RhB removal

Electrocatalytic generation of radicals played important roles in indirect oxidation of contaminants in the 3DER (Zhu et al., 2011). Accordingly, DMPO spin-trapped ESR spectroscopy was used to track the activated radicals formed in 3DER. As shown in Fig. 7, •OOH characterized by seven intensity peaks were detected for GSC-10, GSC-CTs and GSC-10-CTs, which was the product of $\bullet O_2^-$ reacting with H_2O (Wang et al., 2017a):

$$\bullet O_2^- + H_2O \rightarrow \bullet OOH + OH^- \quad (2)$$

The mechanisms for radicals production were distinct for different GSCs. GSC-10 generated radicals while GSC not, that was highly related with the macropores in GSC-10. More catalytic sites interior could participate reactions due to enhanced mass transfer by macropores. Radicals generated by GSC-CTs were mainly due to the increased catalytic components from copper tailings. Therefore, the peak intensity of GSC-10-CTs in ESR spectrum was the strongest by improving mass transfer and catalytic components simultaneously. GSC-10-CTs was efficient catalyst for radicals generation and hence for the indirect oxidation of pollutants.

To demonstrate the contributions of radicals to RhB removal, tertbutyl alcohol was added into the influent as radical scavengers. As shown in Fig. 2e, the removal efficiency of all GSCs decreased to various degrees after quenching the radicals. Especially for GSC-10-CTs, stable treatment efficiency could not be maintained lacking of radicals during long-term operation. Fig. 2f presented the removal efficiency contributed by radicals by subtracting Fig. 2a—e. It was found that the contribution of radicals was less than 10% for GSC-10 in spite of considerable capability of GSC-10 in generating radicals (Fig. 7). The reason might be the excessive adsorption of RhB by GSC-10 (Fig. 2b), leading to the coverage of catalytic sites by the contaminants. The results implied that adsorption and electrocatalysis of contaminants by particle electrodes should be matched in 3DER. The evolution of GSC and GSC-CTs was similar, displaying a trend of first rise then decline. The increased contribution of radicals synchronized with the decreased contribution of adsorption (Fig. 2f). The subsequently declined trend was mainly due to the coverage of catalytic sites. Therefore, roles of radicals in contaminants removal not only depended on radicals generation by GSCs but also being related with mass transfer at the interface of GSCs. Due to the excellent electrocatalytic property and porous structure of GSC-10-CTs, the contributions of radicals kept growing during 14 h operation.

4.2. GSCs of hierarchical-pore structure resist deactivation

The porous structure of the GSCs greatly influenced wastewater treatment performance of 3DER. There appeared significant attenuation in RhB removal efficiency after 8 h treatment for GSC and GSC-CTs (Fig. 2a). Since lacking macropores, RhB was difficult to diffuse into the interior of GSCs. Mass transfer in these GSCs were restricted, only catalytic sites on GSCs surface could participate the electrocatalytic process. Accordingly, these exposed catalytic sites were gradually covered by the contaminants, leading to the reduction in treatment performance with operation time. The poor adsorption of RhB by GSC and GSC-CTs also demonstrated the limited mass transfer of RhB in these GSCs (Fig. 2b). The adsorption capability of GSCs was irrelevant with their BET surface area

(Table 2), but highly depending on the macropores in GSC-10 and GSC-10-CTs. The macropores created by PMMA allowed RhB to migrate into the GSC-10, presenting the strongest adsorption capability (Fig. 2b). However, the weak electrocatalytic property led to accumulation of RhB in GSC-10, and RhB removal efficiency decreased dramatically when catalytic sites were covered by the contaminants. GSC-10-CTs exhibited stable treatment performances due to the hierarchical-pore structure, effectively resisting deactivation of the particle electrodes. Macropores primarily worked as channels for mass transfer (Aschermann et al., 2018), that were essential for the diffusion of RhB into GSC-10-CTs of centimeter-size. Meso- and micropores enlarged specific surface area and therefore incremental catalytic sites were available (Li et al., 2014). Thereafter, micro- and mesopores located interior could participate the catalytic reactions. RhB was continuously removed by GSC-10-CTs because of the hierarchical-pore structure and excellent electrocatalytic property.

4.3. Environmental and economic significance of GSCs

Sewage sludge is an inevitable by-product from wastewater treatment plants produced in large amounts. Fabricating sludge-derived GSCs offers a new strategy for wastes recycling, exhibiting obvious environmental significance. Production of commercial GAC catalysts generally comprise two steps, fabricating GAC from coal/biomass and loading metals such as Pd and Cu on GAC to enhance the catalytic properties (Zhang et al., 2013). In this study, GSCs are fabricated by one-step approach of activation, granulation and carbonization, in-situ utilizing organic matters and metals in sludge and copper tailings. Compared to producing commercial GAC catalysts, PMMA is the main additional chemical which vaporizes in the forms of CO_2/CO during pyrolysis. The metals are free of use during GSCs fabrication, avoiding the secondary pollution of heavy metals. Therefore, we consider that GSCs fabrication is more environmental.

The fabrication cost of GSCs could be evaluated based on sludge-pyrolyzed activated carbon, which is about RMB 620–1240/ton considering transportation, energy consumption, chemicals, and other processes (Bhatnagar et al., 2008). The fabrication procedure of GSCs is similar with sludge-pyrolyzed activated carbon except extra doping 10% PMMA (RMB 15000/ton) and 5% copper tailings (free). Therefore, the finished GSCs products would cost lower than RMB 3000/ton by adding all the expenses, that is much lower than the cost of the cheapest GAC catalysts in the market (about RMB 8000/ton). It is reasonable to conclude that GSCs are cost-effective catalysts for wastewater treatment.

5. Conclusions

In this study, GSCs were fabricated by pyrolyzing the mixture of waste sludge, PMMA and copper tailings, and filled into 3DER as particle electrodes for RhB wastewater treatment. Results indicated that GSC-10-CTs performed the highest removal efficiency and the lowest energy consumption during RhB treatment process. Superior hierarchical-pore structure comprising macro-, meso- and micropores was established in GSC-10-CTs, being more resistant to deactivation during wastewater treatment. PMMA constructed macropores were essential for the mass transfer of RhB into GSCs of centimeter-size. Copper tailings facilitated the formation of meso- and micro-pores during sludge pyrolysis, as well as improving electrochemical activity of GSCs. In addition, the compressive strength of the porous GSC-10-CTs were enhanced in the presence of copper tails, that was crucial to fill into 3DER as particle electrodes. The environmental friendly and cost-effective GSCs might substitute commercial GAC catalysts in the future.

Declaration of competing interest

The authors declare that they have no known competing financial interests or personal relationships that could have appeared to influence the work reported in this paper.

Acknowledgements

The authors wish to thank National Natural Science Foundation of China (51708224) for the support of this study.

Appendix A. Supplementary data

Supplementary data to this article can be found online at https://doi.org/10.1016/j.watres.2019.115016.

References

Aschermann, G., Zietzschmann, F., Jekel, M., 2018. Influence of dissolved organic matter and activated carbon pore characteristics on organic micropollutant desorption. Water Res. 133, 123–131.
Bagreev, A., Bandosz, T.J., Locke, D.C., 2001. Pore structure and surface chemistry of adsorbents obtained by pyrolysis of sewage sludge-derived fertilizer. Carbon 39, 1971-1979.
Bandosz, T.J., Block, K., 2006. Effect of pyrolysis temperature and time on catalytic performance of sewage sludge/industrial sludge-based composite adsorbents. Appl. Catal. B Environ. 67, 77–85.
Bhatnagar, A., Minocha, A.K., Pudasainee, D., Chung, H.K., Kim, S.H., Kim, H.S., Lee, G., Min, B., Jeon, B.H., 2008. Vanadium removal from water by waste metal sludge and cement immobilization. Chem. Eng. J. 144, 197–204.
Contreras Moreno, V., Ledoux, A., Estel, L., Derrouiche, S., Denieul, M.-P., 2017. Valorisation of CO_2 with epoxides: influence of gas/liquid mass transfer on reaction kinetics. Chem. Eng. Sci. 170, 77–90.
East, M., 2016. Physisorption of gases, with special reference to the evaluation of surface area and pore size distribution. Pure Appl. Chem. 38, 25-25.
Feng, H., Zheng, M., Dong, H., Xiao, Y., Hu, H., Sun, Z., Long, C., Cai, Y., Zhao, X., Zhang, H., Lei, B., Liu, Y., 2015. Three-dimensional honeycomb-like hierarchically structured carbon for high-performance supercapacitors derived from high-ash-content sewage sludge. J. Mater. Chem. A. 3, 15225–15234.
Gu, L., Zhu, N., Guo, H., Huang, S., Lou, Z., Yuan, H., 2013. Adsorption and Fenton-like degradation of naphthalene dye intermediate on sewage sludge derived porous carbon. J. Hazard Mater. 246–247, 145–153.
Hadi, P., Xu, M., Ning, C., Sze Ki Lin, C., McKay, G., 2015. A critical review on preparation, characterization and utilization of sludge-derived activated carbons for wastewater treatment. Chem. Eng. J. 260, 895–906.
Hou, B., Han, H., Jia, S., Zhuang, H., Xu, P., Li, K., 2016. Three-dimensional heterogeneous electro-Fenton oxidation of biologically pretreated coal gasification wastewater using sludge derived carbon as catalytic particle electrodes and catalyst. J. Taiwan Inst. Chem. E. 60, 352–360.
Hu, X., Liu, B., Deng, Y., Chen, H., Luo, S., Sun, C., Yang, P., Yang, S., 2011. Adsorption and heterogeneous Fenton degradation of 17α-methyltestosterone on nano Fe_3O_4/MWCNTs in aqueous solution. Appl. Catal. B Environ. 107, 274–283.
Ji, J., Li, X.Y., Xu, J., Yang, X.Y., Meng, H.S., Yan, Z.R., 2018. Zn-Fe-rich granular sludge carbon (GSC) for enhanced electrocatalytic removal of bisphenol A (BPA) and Rhodamine B (RhB) in a continuous-flow three-dimensional electrode reactor (3DER). Electrochim. Acta 284, 587–596.
Kong, L., Xiong, Y., Tian, S., Luo, R., He, C., Huang, H., 2013. Preparation and characterization of a hierarchical porous char from sewage sludge with superior adsorption capacity for toluene by a new two-step pore-fabricating process. Bioresour. Technol. 146, 457–462.
Lee, J.S., Kim, S.I., Yoon, J.C., Jang, J.H., 2013. Chemical vapor deposition of mesoporous graphene nanoballs for supercapacitor. ACS Nano 7, 6047–6055.
Li, D., Qu, Y., Liu, J., He, W., Wang, H., Feng, Y., 2014. Using ammonium bicarbonate as pore former in activated carbon catalyst layer to enhance performance of air cathode microbial fuel cell. J. Power Sources 272, 909–914.
Li, S., Feng, J., Tian, S., Lan, S., Fan, C., Liu, X., Xiong, Y., 2018. Tuning role and mechanism of paint sludge for characteristics of sewage sludge carbon: paint sludge as a new macro-pores forming agent. J. Hazard Mater. 344, 657–668.
Li, X., Li, W.G., Wang, G.Z., Wang, P., Gong, X.J., 2015. Preparation, characterization, and application of sludge with additive scrap iron-based activated carbons. Desalin. Water Treat. 54, 1194–1203.
Li, X., Wu, Y., Zhu, W., Xue, F., Qian, Y., Wang, C., 2016. Enhanced electrochemical oxidation of synthetic dyeing wastewater using SnO_2-Sb-doped TiO_2-coated granular activated carbon electrodes with high hydroxyl radical yields. Electrochim. Acta 220, 276–284.
Liu, H., Hu, H., Luo, G., Li, A., Xu, M., Yao, H., 2013. Enhancement of hydrogen production in steam gasification of sewage sludge by reusing the calcium in lime-conditioned sludge. Int. J. Hydrogen Energy 38, 1332–1341.
Neti, N.R., Misra, R., 2012. Efficient degradation of Reactive Blue 4 in carbon bed

electrochemical reactor. Chem. Eng. J. 184, 23–32.
Sun, H., Chen, T., Kong, L., Cai, Q., Xiong, Y., Tian, S., 2015. Potential of sludge carbon as new granular electrodes for degradation of acid orange 7. Ind. Eng. Chem. Res. 54, 5468–5474.
Tang, S.Q., Zheng, C.M., Zhang, Z.T., 2018a. Effect of inherent minerals on sewage sludge pyrolysis: product characteristics, kinetics and thermodynamics. Waste Manag. 80, 175–185.
Tang, Y., Zheng, X., Ma, W., Wu, P., 2018b. Residues from sewage sludge incineration for ceramic products with potential for zinc stabilization. Waste Manag. 82, 188–197.
Thomas, B.S., Damare, A., Gupta, R.C., 2013. Strength and durability characteristics of copper tailing concrete. Constr. Build. Mater. 48, 894–900.
Wang, C.Y., Zhang, X., Qiu, H.B., Wang, W.K., Huang, G.X., Jiang, J., Yu, H.Q., 2017a. Photocatalytic degradation of bisphenol A by oxygen-rich and highly visible-light responsive $Bi_{12}O_{17}Cl_2$ nanobelts. Appl. Catal. B Environ. 200, 659–665.
Wang, X., Gu, L., Zhou, P., Zhu, N., Li, C., Tao, H., Wen, H., Zhang, D., 2017b. Pyrolytic temperature dependent conversion of sewage sludge to carbon catalyst and their performance in persulfate degradation of 2-Naphthol. Chem. Eng. J. 324, 203–215.
Wei, L., Guo, S., Yan, G., Chen, C., Jiang, X., 2010. Electrochemical pretreatment of heavy oil refinery wastewater using a three-dimensional electrode reactor. Electrochim. Acta 55, 8615–8620.
Wen, H., Gu, L., Yu, H., Qiao, X., Zhang, D., Ye, J., 2018. Radical assisted iron impregnation on preparing sewage sludge derived Fe/carbon as highly stable catalyst for heterogeneous Fenton reaction. Chem. Eng. J. 352, 837–846.
Xia, Y., Zeng, Y.-P., Jiang, D., 2011. Mechanical and dielectric properties of porous Si_3N_4 ceramics using PMMA as pore former. Ceram. Int. 37, 3775–3779.
Xie, R., Jiang, W., Wang, L., Peng, J., Chen, Y., 2013. Effect of pyrolusite loading on sewage sludge-based activated carbon in Cu(II), Pb(II), and Cd(II) adsorption. Environ. Prog. Sustain. 32, 1066–1073.
Xu, L., Song, X., 2015. A novel Ti/antimony-doped tin oxide nanoparticles electrode prepared by screen printing method and its application in electrochemical degradation of C.I. Acid Red 73. Electrochim. Acta 185, 6–16.
Yang, J.K., Xu, X.Y., Liang, S., Guan, R.N., Li, H.S., Chen, Y., Liu, B.C., Song, J., Yu, W.B., Xiao, K.K., Hou, H.J., Hu, J.P., Yao, H., Xiao, B., 2018. Enhanced hydrogen production in catalytic pyrolysis of sewage sludge by red mud: thermogravimetric kinetic analysis and pyrolysis characteristics. Int. J. Hydrogen Energy 43, 7795–7807.
Yang, X., Xu, G.R., Yu, H.R., Zhang, Z., 2016. Preparation of ferric-activated sludge-based adsorbent from biological sludge for tetracycline removal. Bioresour. Technol. 211, 566–573.
Yuan, S.J., Dai, X.H., 2016. Efficient sewage sludge-derived bi-functional electrocatalyst for oxygen reduction and evolution reaction. Green Chem. 18, 4004–4011.
Zhang, C., Jiang, Y.H., Li, Y.L., Hu, Z.X., Zhou, L., Zhou, M.H., 2013. Three-dimensional electrochemical process for wastewater treatment: a general review. Chem. Eng. J. 228, 455–467.
Zheng, T., Wang, Q., Shi, Z., Fang, Y., Shi, S., Wang, J., Wu, C., 2016. Advanced treatment of wet-spun acrylic fiber manufacturing wastewater using three-dimensional electrochemical oxidation. J. Environ. Sci. 50, 21–31.
Zhu, X., Ni, J., Xing, X., Li, H., Jiang, Y., 2011. Synergies between electrochemical oxidation and activated carbon adsorption in three-dimensional boron-doped diamond anode system. Electrochim. Acta 56, 1270–1274.